JCTC Journal of Chemical Theory and Computation

Article

pubs.acs.org/JCTC

A Polarizable QM/MM Explicit Solvent Model for Computational Electrochemistry in Water

Lee-Ping Wang and Troy Van Voorhis*

Department of Chemistry, Massachusetts Institute of Technology, 77 Massachusetts Avenue, Cambridge, Massachusetts 02139, United States

ABSTRACT: We present a quantum mechanical/molecular mechanical (QM/MM) explicit solvent model for the computation of standard reduction potentials E_0. The QM/MM model uses density functional theory (DFT) to model the solute and a polarizable molecular mechanics (MM) force field to describe the solvent. The linear response approximation is applied to estimate E_0 from the thermally averaged electron attachment/detachment energies computed in the oxidized and reduced states. Using the QM/MM model, we calculated one-electron E_0 values for several aqueous transition-metal complexes and found substantially improved agreement with experiment compared to values obtained from implicit solvent models. A detailed breakdown of the physical effects in the QM/MM model indicates that hydrogen-bonding effects are mainly responsible for the differences in computed values of E_0 between the QM/MM and implicit models. Our results highlight the importance of including solute−solvent hydrogen-bonding effects in the theoretical modeling of redox processes.

1. INTRODUCTION

Electrochemistry, defined as electron transfer between a conducting electrode and a molecule or ion in solution, allows us to explore the fascinating array of oxidation−reduction (redox) chemistry underlying a great many processes in organic,[1−3] inorganic,[4−7] and biological chemistry.[8−11] Additionally, electrochemical processes play an indispensable role in the fields of energy storage and conversion as the underlying mechanism for the operation of batteries[12,13] and the pathway for conversion of electrical energy into chemical fuels.[14] In recent years, with the assistance of theoretical models and powerful computers, simulations have started to play an increasingly important role in the understanding of biochemical and energy-related redox processes.[15−22]

The fundamental electrochemical property of a molecule and its associated solvent is the standard reduction potential E_0, which is proportional to the free energy of reduction of the molecule in solvent and referenced to that of a standard electrochemical reaction, e.g., proton reduction at the normal hydrogen electrode (NHE). The solute changes its electronic state during this process by virtue of gaining an electron, and the solvent responds mostly via polarization, either by electron redistribution or molecular reorientation; a model for redox processes must then account for both the electronic structure of the solute and the solvent response.

In general, the electronic structure of the solute is describable by the same quantum chemical methodologies commonly used in gas-phase calculations. In practice, density functional theory (DFT) is often used to describe the electronic structure of the solute, although fully ab initio methods, such as Hartree−Fock,[23,24] multiconfigurational self-consistent field,[25,26] second-order perturbation theory,[27,28] and coupled-cluster theory[29−32] have also been applied. For relatively large systems (i.e., >50 atoms), DFT provides a good compromise between accuracy and computational cost. General-purpose density functionals, such as B3LYP[33] and PBE,[34] have intrinsic errors on the order of 100−300 mV (about 2−7 kcal/mol) for reaction energies of small molecules[35−37] and for gas-phase ionization potentials (IPs) and electron affinities (EAs) of a wide range of molecules,[38−40] including transition-metal complexes;[41−44] this provides a rough upper limit for the accuracy of E_0 computations that utilize these functionals.

The other required component for computation of E_0 is an accurate description of the solvent. Solvent models can be broadly categorized into explicit and implicit solvent models, which are distinguished by whether the model contains any discrete solvent molecules. Implicit solvent models (ISMs) represent the solvent using a dielectric continuum with the solvent's experimentally determined dielectric constant, which generates a reaction field in response to the solute electron density. Perhaps the earliest such ISM is the Born model[45] which describes the dielectric energy of a spherical ion placed in a spherical cavity surrounded by the dielectric continuum. This was refined by the Kirkwood−Onsager model[46,47] which includes the dielectric energy of the higher-order multipole moments of the solute in a spherical cavity. More recent models place the solute into a shaped cavity constructed from an electronic density isosurface[48] or the union of small atom-centered spheres.[49] The solvation energy is then obtained by any of several numerical methods, including solving the Poisson−Boltzmann equation on a grid in space,[50] placing screening charges on the cavity surface,[49,51] or with an integral equation formalism.[52] Modern implementations of implicit solvent models include but are not limited to IEF-PCM,[52] C-PCM,[23] COSMO,[49] and the SMx series;[53] these models are highly popular due to their simplicity and low cost.[54] Within an implicit solvent framework, London dispersion[55] and excluded volume effects[56,57] can also be described in addition to the dielectric response.

Received: May 19, 2011
Published: January 6, 2012

   dx.doi.org/10.1021/ct200340x | J. Chem. Theory Comput. 2012, 8, 610−617

Simple protocols exist for the computation of E_0 in ISMs,[58−65] and highly accurate results have been obtained using DFT/ISM for a variety of organic molecules[60,64,66−68] and transition-metal complexes[60,65,69] in a variety of solvents. However, one intuitively expects the validity of ISMs to vary from system to system as they do not describe many aspects of the solute−solvent interaction including solute−solvent correlations, charge transfer to solvent, or hydrogen-bonding effects. Thus, for example, ISMs provide an excellent description of redox potentials in organic solvents.[60] However, in this paper we are interested in the prediction of accurate reduction potentials for transition metals in water, and the quality of ISM results here is quite mixed. For example, DFT/ISM computation of E_0 for transition-metal aqua complexes suffer from large errors unless a second solvation shell of water molecules is explicitly included in the electronic structure calculation.[59,61,70] Chiorescu and co-workers[69] reported a standard error of 200−600 mV for ISM computations of E_0 for a large number of ruthenium transition-metal complexes and found the largest errors when the solute is highly charged and contains many hydrogen-bond donors. Recent work in the Truhlar and Goddard groups based on population analysis suggested that the second explicit solvation shell affects E_0 by charge transfer to the solute,[71,72] but energy decomposition analyses in the Head-Gordon and Gao groups indicated that population analysis often overestimates the amount of charge transfer in hydrogen bonds.[73−75] To improve the accuracy of ISMs, custom density functionals have been designed which contain empirical fitting to solvent effects;[76−78] highly detailed solvent models tailored to a wide range of physical properties of specific solvents have also been developed.[53]

Explicit solvent models have a far greater capacity to capture the physical details of the solvent. As an example, the SPC/E[79] classical water model not only correctly reproduces the zero-frequency dielectric constant of water but also describes the fine-grained structure of water and describes hydrogen-bonding effects empirically using a combination of electrostatic point charges and van der Waals interactions. Classical explicit solvent molecules can be combined with a DFT treatment of the solute in a quantum mechanical/molecular mechanical (QM/MM) framework[80−83] (Figure 1), or the entire system can be treated quantum mechanically. A downside to these models is an immense increase in computational cost associated with thermally sampling the many configurations of the explicit solvent. Despite these difficulties, explicit solvent models have been applied to compute E_0 for systems of small size, including transition-metal aqua complexes[84−86] and small organic molecules;[87] in these studies both solute and solvent were treated using DFT, with the exception of ref 85, which uses QM/MM. QM/MM models have also been applied to compute E_0 for biological cofactors bound to enzymes[18,20,88−92] where the highly heterogeneous environment of the enzyme active site demands an explicit solvent treatment.

The main purpose of this article is to provide a general protocol for computing E_0 in aqueous solution using QM/MM explicit solvent and a full dynamical treatment of both solute and solvent degrees of freedom. We begin by briefly summarizing the methodologies for ISM and explicit solvent models associated with computing E_0. We present a polarizable QM/MM explicit solvent model which significantly improves the accuracy of E_0 calculations for transition-metal aqua complexes in water. We provide a detailed analysis of the various physical effects in the QM/MM model in order to pinpoint the source of the dramatic differences between the ISM and QM/MM results, and by process of elimination, we conclude that the explicit account of hydrogen-bonding effects is primarily responsible for the improved performance of the QM/MM model. Finally, we summarize the strengths and weaknesses of our model and suggest avenues for further improvement and applications.

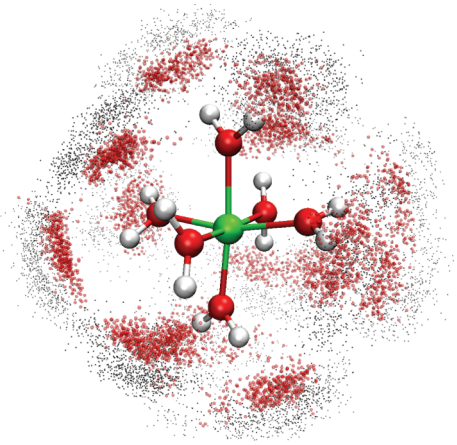

Figure 1. Illustration of a QM/MM simulation of a $[Fe(H_2O)_6]^{3+}$ complex showing QM solute (green, Fe; red, O; white, H) and superimposed positions of MM solvent molecules (red, O; black, H). The geometry of the solute is held fixed. The positions of MM atoms are an approximate representation of the probability distribution of nuclear positions, and the short-range solvent structure (interpreted as a consequence of solute−solvent hydrogen bonding) is visible.

2. THEORY

The general procedure for computation of standard reduction potentials E_0 is given here. E_0 is related to the standard reduction free energy in solution by

$$-FE_0 = \Delta G^{EA}_{(sol)} \quad (1)$$

where $\Delta G^{EA}_{(sol)}$ is the free energy change associated with reduction at standard conditions and F is the Faraday constant. To obtain potentials referenced to NHE, the absolute potential of the NHE is subtracted from the computed value of E_0; in this work, we use a value of 4.43 V,[93] although values ranging from 4.24[94] to 4.73 V[95] are also given in the literature. The implicit and explicit solvent models contain major technical differences in the computation of $\Delta G^{EA}_{(sol)}$, so the following two subsections will separately describe the theories corresponding to the two models.

2.1. Implicit Solvent Calculation of Standard Reduction Potentials. In ISMs, $\Delta G^{EA}_{(sol)}$ is the difference between several components of the Gibbs free energy computed separately for the reduced and oxidized species:[59,60]

$$\Delta G^{EA}_{(sol)} = \Delta G^{EA}_{(g)} + \Delta\Delta G_{solv} \quad (2)$$

$$\Delta G^{EA}_{(g)} = \Delta E_{SCF} + \Delta H^{T} - T\Delta S_{(g)} \quad (3)$$

Here E_{SCF} and ΔG_{solv} are the electronic energy and free energy of solvation, respectively. In ISMs, the space surrounding the solute is filled with a dielectric continuum which generates a reaction field in response to the solute electron density. This interaction yields the solvation free energy ΔG_{solv}, and the difference in ΔG_{solv} values for the two redox states is given by

dx.doi.org/10.1021/ct200340x | J. Chem. TheoryComput. 2012, 8, 610−617

$\Delta\Delta G_{solv}$. Since the reaction field and the solute electronic structure depend on one another, both entities are simultaneously iterated to self-consistency, and the sum of electronic and solvation free energies $E_{SCF} + \Delta G_{solv}$ is computed together. H^T and $-TS$ are the gas-phase enthalpy and entropy contributions to the Gibbs free energy, respectively. These terms are obtained from the translational and rotational degrees of freedom as well as the normal modes of the molecule from a frequency calculation.

Since ISMs allow one to obtain all components of the free energy for a given oxidation state from a single electronic structure calculation, it is computationally efficient and thus generally preferred for calculations of E_0. The model makes several important assumptions. One major assumption is that the solute is well described by a continuum dielectric; the validity of this assumption depends on the strength of the solute−solvent interaction and is more likely to break down when solute−solvent hydrogen bonding is present. ISMs further assume that a mean-field model is appropriate; the solute sees the average reaction field as opposed to having the solute wave function and solvent polarization respond instantaneously to one another. Furthermore, the flexibility of the solute is only treated in terms of its harmonic vibrations around the minimum-energy geometry. These assumptions of ISMs can be investigated by using explicit solvent models which provide a dynamical treatment and a highly detailed description of the solvent.

2.2. QM/MM Calculation of Standard Reduction Potentials. In order to obtain the free energy difference ΔG between oxidized and reduced states in the context of QM/MM molecular dynamics simulations, we use the formalism of thermodynamic integration (TI).[96] Within this framework, we first write down a superposition of the system's potential energy function in its reactant and product states using a tunable parameter λ:

$$E(\lambda) = \lambda E_{ox} + (1 - \lambda)E_{red} \tag{4}$$

where we recover the reduced state when $\lambda = 0$ and the oxidized state when $\lambda = 1$. The goal is to find the free energy difference between the two states: $\Delta F = F(\lambda = 1) - F(\lambda = 0)$.

Differentiating the relation between the partition function Z and the free energy with respect to λ gives the following relationship between the *free* energy derivative and the *potential* energy derivative:

$$\begin{aligned}\frac{dF}{d\lambda} &= \frac{d}{d\lambda}k_b T \log Z \\ &= \frac{1}{Z}\sum_i \frac{dE_i(\lambda)}{d\lambda}e^{-\beta E_i(\lambda)} \\ &= \left\langle \frac{dE(\lambda)}{d\lambda} \right\rangle\end{aligned} \tag{5}$$

Thus, the free energy derivative at a given value of λ is given by thermally averaging the potential energy derivative using the canonical ensemble corresponding to $E(\lambda)$. The potential energy derivative is given by the vertical energy gap (EG) between reactant and product states:

$$\frac{dE(\lambda)}{d\lambda} = E_{ox} - E_{red} \tag{6}$$

By this formalism, the free energy derivative $dF/d\lambda$ can be evaluated using sampling techniques such as the Metropolis algorithm.[97] TI consists of evaluating $dF/d\lambda$ at several values of λ between 0 and 1 and then numerically integrating to evaluate ΔF:

$$\Delta F = \int_0^1 d\lambda \frac{dF}{d\lambda} = \int_0^1 d\lambda \left\langle \frac{dE}{d\lambda} \right\rangle \tag{7}$$

Note that intermediate λ values between 0 and 1 correspond to unphysical systems, and carrying out these simulations can be a nontrivial task especially when the reactant and product have different numbers of atoms, as is the case in protonation/deprotonation reactions.[20,87,90,92]

In the linear response (LR) approximation, the free energy derivative $(dF/d\lambda)$ is assumed to be linear in λ, and ΔF can be evaluated by thermally averaging the vertical EG at the reduced and oxidized states (i.e., at $\lambda = 1$ and 0):

$$\begin{aligned}\Delta F &= \int_0^1 d\lambda \left\langle \frac{dE}{d\lambda} \right\rangle \\ &= \frac{1}{2}(\langle E_{ox} - E_{red}\rangle_{ox} + \langle E_{ox} - E_{red}\rangle_{red})\end{aligned} \tag{8}$$

Note that the LR approximation can be tested by evaluating $(dF/d\lambda)$ at intermediate λ values and performing TI.[87] In this Article, we have used the LR approximation throughout; some validation for the LR approximation is provided in ref 85, in which full TI was performed on two transition-metal complexes using a related protocol.

3. COMPUTATIONAL METHODS

3.1. Implicit Solvent Model. All DFT/ISM calculations were performed with the B3LYP density functional[33] and the conductor-like screening model (COSMO)[49] as implemented within TURBOMOLE, version 5.10.[98] The optimized atomic radii were used where available,[99] and Bondi's radii[100] were used for metal atoms. Geometry optimizations were performed in the gas phase using the SDD basis/pseudopotential combination[101] for metals and the TZVP basis[102] for all other atoms; gas-phase frequency calculations were performed at the optimized geometries using the same level of theory. Single-point energies in the solvent phase were computed at the gas-phase optimized geometries using SDD for metals and cc-pVTZ[103] for all other atoms. The unrestricted spin formalism was used at all times, and the multiplicities of all complexes were set to the experimentally determined values.

3.2. QM/MM Model. To prepare the simulation cell, the solute geometry was optimized in the gas phase and placed in the center of a 3.7 nm cubic box; ≈1720 explicit solvent water molecules, modeled using the SPC/E force field, were then added to fill the box. The solute−solvent interaction was given by a QM/MM interaction potential as described in refs 81 and 82. The QM solute was not treated using periodic boundary conditions and interacts only with the nearest periodic image of the MM solvent molecules. Long-range electrostatic interactions within the MM region were treated using the particle-mesh Ewald method using a cutoff of 9.0 Å. The Lennard-Jones (LJ) parameters for the solute were taken from UFF,[104] except the R_{min} parameter on the solute hydrogens which was adjusted to 0.15 Å; this value was determined by running a QM/MM simulation with just one QM water molecule and optimizing the LJ radius of the QM hydrogens to reproduce the typical hydrogen bond length of 1.7 Å between MM waters. Dynamics

were performed in the NVT ensemble with a Nosé−Hoover thermostat; we used a time step of 1.0 fs, the SHAKE constraint algorithm[105] was applied to the MM water molecules, and the solute was centered in the simulation cell at every time step. For each complex in each oxidation state, the first 5 ps were used for thermal equilibration, and at least 20 ps of QM/MM dynamics were generated in total.

We extracted configurations (snapshots) from the molecular dynamics trajectories at 40 fs intervals to perform EG calculations. EG calculations were equivalent to computing the vertical IP (EA) at simulation snapshots corresponding to the reduced (oxidized) species; the result of the IP calculation was multiplied by −1 to obtain the EG. The average EG from the oxidized and reduced trajectories were then combined in eq 8 to obtain the free energy of reduction, $\Delta G^{EA}_{(sol)}$.

It is important to note here that the SPC/E water model implicitly accounts for solvent polarizability in equilibrium molecular dynamics but cannot capture electronic polarization effects that accompany vertical electron detachment/attachment. We decided to explicitly add electronic polarization of the solvent in the form of polarizable Drude particles[106,107] in the EG calculations. For these calculations, a single Drude particle with polarizability 1.0425 Å was attached to each water oxygen; the value of the parameter was taken from ref 107 and reflects the refractive index of liquid water. To ensure that the Drude particles account only for the electron detachment/attachment events, we only included Drude polarization in the nonequilibrium term in the EG; that is, when we calculated the EG for snapshots sampled from the E_{red} ensemble, Drude particles were added for calculations of E_{ox} and vice versa.

Recent studies have shown that the choice of water model has a profound effect on the mean electrostatic potential (ESP) of the simulation cell with respect to vacuum.[108] Furthermore, the mean ESP may be affected by a liquid−vacuum interface that is present in the experimental measurement but not accounted for by the simulations.[109] To investigate, we computed the ESP on a grid inside the simulation cell following procedures outlined in ref 108 and found an average of $\approx -0.5 \pm 0.1$ V for the SPC/E simulation cell; this could potentially introduce a bias of 0.5 V into our results. However, upon closer examination, the largest contributions to the ESP came from regions close to the MM point charges (<1 Å) which do not overlap appreciably with the QM electron density; when regions near the MM atoms (<1 UFF radius) were excluded from the calculation, the average ESP became 0.0 ± 0.1 V. We also compared simulations with and without an explicit interface to vacuum and found a difference in the average ESP of 0.1 ± 0.1 V, suggesting that the surface dipole effect from the liquid−vacuum interface is relatively minor, in agreement with previous calculations.

All QM/MM calculations were performed using the CHARMM (version c34b1)[110]/Q-Chem (version 4.0)[111] interface.[112] The TZVP all-electron basis set was used for all atoms. In the polarizable QM/MM calculations, the Drude particle positions and Kohn−Sham wave function were self-consistently determined using a specialized dual convergence procedure[113] that updates both quantities simultaneously to minimize computational cost.

4. RESULTS

We chose a set of small organic molecules, metallocene ("sandwich") complexes, and octahedrally coordinated transition-metal complexes from ref 60 to act as our control set for the ISM; they comprise a fairly diverse set of redox-active small molecules in a variety of solvents for which ISMs are known to provide a reasonably good description.

We also put together a test set of nine first-row transition-metal complexes in aqueous solvent, two of which also belong to the control set; E_0 was computed using both ISM and QM/MM techniques for each complex in this set. These complexes are: $[Ti(H_2O)_6]^{3+}$, $[V(H_2O)_6]^{3+}$, $[Cr(H_2O)_6]^{3+}$, $[Mn(H_2O)_6]^{3+}$, $[Fe(H_2O)_6]^{3+}$, $Fe[(CN)_6]^{3-}$, $[Co(H_2O)_6]^{3+}$, $[Co(NH_3)_6]^{3+}$, and $[Cu(H_2O)_6]^{3+}$. The experimental values of E_0 for these nine complexes are given in the most recent edition of the CRC Handbook.[114] The nine aqueous transition-metal complexes were chosen because they satisfied the following conditions and were desirable for a study of this type: (1) they reversibly underwent one-electron redox reactions without undergoing any concomitant chemical reactivity; (2) they are sufficiently small that expensive QM/MM simulations were relatively tractable; and (3) their experimental E_0 values are accurately known.

4.1. Standard Reduction Potentials in ISM. Using the ISM, we reproduced the results from ref 60 for the control set (Figure 2, scatter plot in gray). However, the result using the same methodology was generally poor for the test set of aqueous transition-metal complexes. The seven $[M(H_2O)_6]^{3+}$ complexes had a particularly large systematic error, where the ISM consistently overstimated E_0 by over 1.62 V (Figure 2, scatter plot in blue); the correct periodic trend was still reproduced with a correlation of >0.98.

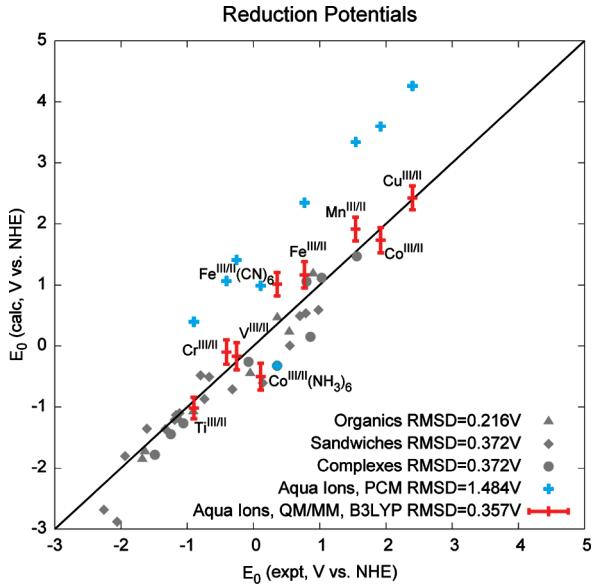

Figure 2. Calculated values of E_0 plotted against experiment. Gray: ISM calculations of E_0 for molecules chosen from ref 60 (organic molecules, triangles; sandwich complexes, diamonds; octahedral complexes, circles). Blue crosses: ISM calculations performed on aqueous transition-metal complexes. Red crosses: QM/MM calculations performed on aqueous transition-metal complexes.

4.2. Standard Reduction Potentials in QM/MM Model. We recomputed E_0 using the QM/MM model (Figure 2, scatter plot in red). In these simulations, the QM region consisted of the transition-metal atom and its six ligands, and the solvent was treated classically. Zero-point vibrational effects, which contributed <0.05 V in the ISM calculations, were ignored. Using the QM/MM model, we found a dramatic

dx.doi.org/10.1021/ct200340x | J. Chem. TheoryComput. 2012, 8, 610−617

improvement in the agreement of our computed values with experiment; the root-mean-square (rms) deviation from experiment dropped by 1.6 V to 0.3 V, and the systematic error for the $[M(H_2O)_6]^{3+}$ ions was nearly eliminated. In fact, all of the cations with a +3 charge underwent a similar shift in their E_0 values when QM/MM was used. The difference between ISM and QM/MM E_0 values for these eight complexes was -1.49 ± 0.24 V. The $Fe[(CN)_6]^{3-}$ ion, the only anion for which QM/MM E_0 values were computed in this work, had a shift in the opposite direction of +1.33 V.

We also estimated the dependence of E_0 on the density functional. In these calculations, the snapshots generated from B3LYP QM/MM were used, and the functional was only varied when calculating the EG. The deviations of the calculated E_0 values from experiment are given in Figure 3. The functionals

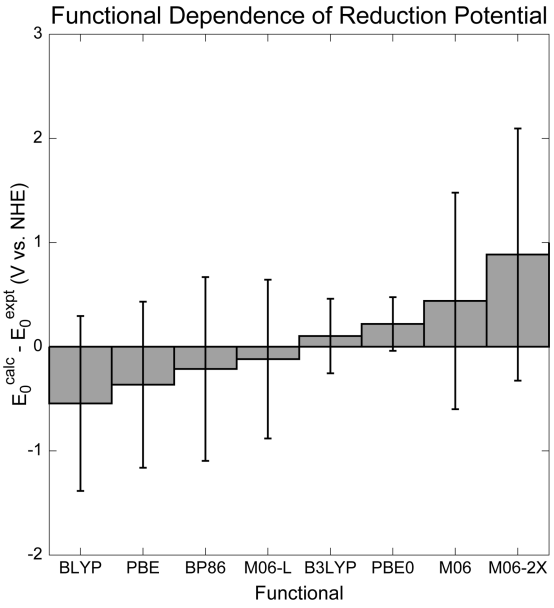

Figure 3. Mean and standard deviation of differences between calculated E_0 values and experimental measurements. Functionals are ordered by mean error, and a correlation between mean error and fraction of Hartree–Fock exchange is observed.

are ordered by their average deviation from experiment, and we can observe a strong correlation between the mean error and the percent of exact exchange in the functional (BLYP, PBE, BP86, M06-L 0%; B3LYP 20%; PBE0 25%; M06 27%; M06-2X 54%.) This correlates with the documented trend for calculated gas-phase IPs of transition-metal atoms to increase with the fraction of exact exchange[42,44,115,116] and confirms the usefulness of using internal references for E_0 computations using different functionals as suggested in ref 65. We also observed that the standard deviation of the error is much larger for functionals with much less or much more exact exchange compared to B3LYP and PBE0; this reflects earlier reports that density functionals with 20–30% exact exchange gave the most accurate gas-phase IP values of transition-metal complexes, whereas functionals with significantly more or less exact exchange were much less accurate.[115,116] In the current study, we judged PBE0 to give the most accurate energy gaps out of all functionals tested, and we speculate that the results may be further improved if PBE0 were used for the QM/MM dynamics as well.

5. DISCUSSION

The significant difference between standard reduction potentials computed using ISM and QM/MM stems from the different physical descriptions of the solvent. The QM/MM description contains many physical effects that are absent in ISMs, including solute flexibility, solute–solvent correlation, and hydrogen bonding. Furthermore, there is a possibility that the errors in ISM are a consequence of incorrect parametrization of the atomic radii. In this section, we present a detailed analysis of the different physical effects in the QM/MM model and their estimated contributions to E_0. We found that solute flexibility and dispersion effects contribute a relatively small amount to E_0. Some of the analyses required customized QM/MM simulations, which were carried out for the $[Fe(H_2O)_6]^{3+}$ complex as a case study. The relevant values of E_0 for this complex are 2.35 V (calculated, ISM), 1.17 V (calculated, QM/MM), and 0.77 V (experiment).

5.1. Atomic Radii in ISM. The most important parameters in a ISM are the dielectric constant of the solvent and the solute atomic radii. While the dielectric constant is fixed, the choice of atomic radii is not entirely unambiguous, and there are several sets of atomic radii, including UFF radii,[104] Bondi's radii,[100] and the optimized radii in TURBOMOLE.[99] We tested the effect of changing the hydrogen radii on the ISM E_0 values for the seven $[M(H_2O)_6]^{3+}$ complexes and found that decreasing the hydrogen radii from 1.3 to 0.7 Å changed the average deviation from experiment from +1.62 to +0.61 V (lowering the radii further had no effect as the hydrogen radii were completely contained within the oxygen radii).

Decreasing the hydrogen radii for other molecules had a much smaller effect; the change in E_0 never exceeded 0.2 V when the hydrogen radii were eliminated from ferrocene and the organics. Thus, it seemed that the transition-metal aqua complexes were especially sensitive to the parametrization of hydrogen radii. Nevertheless, a sizable systematic deviation from experiment still existed when the hydrogen radii were tuned to zero, and from this, we concluded that the residual errors associated with ISM computations for these systems were not a consequence of improper parametrization but rather the inability of the ISM to describe important physical effects.

5.2. Solute Flexibility. A major difference between the ISM and QM/MM models is the treatment of solute dynamics. ISM approximates the dynamics of the solute using harmonic vibrations about the minimum-energy geometry, while QM/MM provides a full dynamical treatment. The harmonic approximation may be valid for solutes with mostly stiff degrees of freedom (e.g., anthracene, $Ru(bpy)_3$, or $Fe(CN)_6$), but it is not an appropriate description for more flexible solutes with more complex conformational changes. In fact, the QM/MM simulations indicated a significant degree of torsional freedom for the aqua ligands on the $[M(H_2O)_6]^{3+}$ complexes, so it is conceivable that solute flexibility effects could have a noticeable effect on E_0.

To investigate, we ran a QM/MM trajectory for the $[Fe(H_2O)_6]^{3+}$ complex with the solute fixed at the gas-phase optimized geometry and calculated E_0 using the same LR approximation. With the solute fixed, we computed a value of 1.07 V for E_0; this constituted a 0.10 V difference from the result obtained from fully flexible dynamics. This is very small when compared to the 1.18 V difference between the ISM and QM/MM calculations; from this, we concluded that the solute flexibility has a relatively minor impact on E_0 for these

complexes. In fact, an accurate estimation of the size of the effect may not be possible from this study due to the statistical errors of ≈0.20 V in the QM/MM calculations. We do not expect our result to hold for all redox systems, especially those with intramolecular hydrogen bonds or multiple conformations (proteins being a prime example).

5.3. Solute−Solvent Correlation. The QM/MM model accounts for temporal correlations between the positions and orientations of solvent water molecules and the solute electron density, but ISM cannot describe them as it is a mean-field model. To investigate, we performed an approximate mean-field QM/MM E_0 calculation on the frozen $[Fe(H_2O)_6]^{3+}$ complex. In this simulation, correlations on time scales smaller than 10 ps were removed by averaging the electrostatic field over 50 snapshots in a 10 ps window. This procedure only removes correlation to first order, as the snapshots themselves were generated using full dynamics, in contrast to fully self-consistent methods.[83,85] The Drude particles were turned off for this test; this also introduces a large shift in the reduction potential, so the results reported in this section are only intended to estimate the size of correlation effects.

When the correlation effects were removed, the computed value of E_0 increased from 3.18 to 3.42 V. This indicates that correlations contribute about 0.24 V, a minor effect when compared to the difference of 1.18 V between the ISM and QM/MM models and within the statistical error bars. In these simulations, the E_0 values were >2 V higher compared to the actual QM/MM results due to the absence of Drude particles; this illustrates the importance of including electronic (fast) polarization in calculations of E_0 and reiterates the need for polarizable force fields in this type of QM/MM model.

5.4. Hydrogen-Bonding Effects. In the QM/MM model, electrostatic interactions between the solvent water molecules and the ligands of the solute give rise to short-range structuring of the second solvation shell and heterogeneous polarization of the solute electron density. These effects are not captured by ISMs, and it is natural to associate these interactions with hydrogen bonding, and we will typically make that association in what follows. By eliminating dispersion and solute flexibility effects, we arrived at the conclusion that short-range solvent structure, i.e., hydrogen-bonding effects, are mainly responsible for the difference between our ISM and QM/MM computed values of E_0.

We note that hydrogen-bonding effects can also be treated using cluster-continuum models that explicitly include the second solvation shell in the quantum calculation;[59,61,70] in these studies, adding the second shell dramatically improves agreement with experiment. These cluster-continuum models allow some charge transfer to take place between the second solvation shell and the solute,[71,72] a feature that is absent in the QM/MM model. The ability of our QM/MM model to reproduce the experimental results seems to suggest that hydrogen-bonding effects on E_0 can be appropriately described using classical electrostatics without the need to invoke charge transfer; the relative contributions of electrostatics and the charge-transfer effects to computed values of E_0 are a topic worthy of further study. We also note that a fully explicit solvent model has the advantage that larger, less symmetric solutes can be treated on the same footing without having to carefully define a second solvation shell.

6. CONCLUSIONS

In this Article we presented a QM/MM model for computing standard reduction potentials in explicit solvent. Our model uses a combination of DFT and a polarizable force field for computing energy gaps associated with vertical electron attachment/detachment. The linear response approximation is applied to estimate the free energy of reduction from the thermally averaged energy gaps in the oxidized and reduced states. Using this model, we computed E_0 for a series of aqueous transition-metal complexes and obtained very good agreement with experimental results.

In an effort to locate the source of the dramatically different results between the ISM and QM/MM models, we investigated the different physical effects in the two models as possible contributing factors. We were able to make the following conclusions:

- ISM calculations for transition-metal aqua complexes are especially sensitive to the choice of hydrogen radii parameters. However, the errors associated with the ISM are not solely caused by poor parameter choice but also stem from physical effects missing from the model.
- Solute flexibility effects contribute a relatively small amount to E_0 calculated using the QM/MM model (≈ 0.1 V) for the transition-metal aqua complexes, which is smaller than the statistical noise.
- Dispersion effects contribute a relatively small amount to E_0 calculated using the QM/MM model (≈ 0.2 V).
- By process of elimination, the largest physical effect responsible for the differences between the QM/MM and ISMs is due to short-range solvent structure, most likely induced by solute−solvent hydrogen bonding.

We conclude with some caveats of the QM/MM model along with proposed improvements and extensions. The treatment of electronic polarizability in this study was not ideal; electronic polarizability was implicit in the equilibrium MD simulations yet explicitly needed for computing the vertical energy gaps. A fully polarizable QM/MM MD simulation may deliver a more satisfactory solution. This would treat both equilibrium and ionized electronic states on the same footing and also allow us to study fluctuations of the energy gap for the purpose of determining Marcus reorganization energies and corrections to the LR approximation.

As with all solvent models, proper calibration and parametrization is essential. A classical explicit solvent model offers a lot of flexibility in its force field parameters, and these parameters must be chosen such that the model properly reproduces important bulk properties of the solvent including but not limited to the dielectric constant. The empirical van der Waals interaction in the QM/MM Hamiltonian must also be parametrized to properly describe the London dispersion forces between solute and solvent; this is a possible application for automatic force matching methods.[117]

Finally, while the aqueous transition-metal complexes presented here offer a reliable benchmark set for testing the QM/MM model, the vast majority of redox processes in aqueous solution are accompanied by interesting chemistry, such as proton transfer and dimerization. Any reaction chemistry that accompanies redox events must be accounted for in the QM/MM model, and this also poses questions for the validity of linear response. Aqueous systems that undergo reversible proton-coupled electron transfer,[87] including phe-

nols, quinones, anilines and other small organics, will be studied in a future report.

AUTHOR INFORMATION

Corresponding Author

*E-mail: tvan@mit.edu.

Notes

The authors declare no competing financial interest.

ACKNOWLEDGMENTS

This work was funded by ENI SpA as part of the Solar Frontiers Research Program. We thank Michiel Sprik for providing much helpful insight and discussion.

REFERENCES

(1) Arends, I. W. C. E.; Sheldon, R. A.; Wallau, M.; Schuchardt, U. *Angew. Chem., Int. Ed.* **1997**, *36*, 1144−1163.
(2) Connelly, N. G.; Geiger, W. E. *Chem. Rev.* **1996**, *96*, 877−910.
(3) Chen, X. M.; Tong, M. L. *Acc. Chem. Res.* **2007**, *40*, 162−170.
(4) Lever, A. B. P. *Inorg. Chem.* **1990**, *29*, 1271−1285.
(5) Beer, P. D. *Adv. Inorg. Chem.* **1992**, *39*, 79−157.
(6) Hill, C. L.; Prossermccartha, C. M. *Coord. Chem. Rev.* **1995**, *143*, 407−455.
(7) Noodleman, L.; Peng, C. Y.; Case, D. A.; Mouesca, J. M. *Coord. Chem. Rev.* **1995**, *144*, 199−244.
(8) Stamler, J. S.; Singel, D. J.; Loscalzo, J. *Science* **1992**, *258*, 1898−1902.
(9) Gray, H. B.; Winkler, J. R. *Annu. Rev. Biochem.* **1996**, *65*, 537−561.
(10) McEvoy, J. P.; Brudvig, G. W. *Chem. Rev.* **2006**, *106*, 4455−4483.
(11) Dempsey, J. L.; Winkler, J. R.; Gray, H. B. *Chem. Rev.* **2010**, *110*, 7024−7039.
(12) Tarascon, J. M.; Armand, M. *Nature* **2001**, *414*, 359−367.
(13) Nazri, G.; Pistoia, G. *Lithium Batteries: Science and Technology*; Springer: New York, 2009.
(14) Lewis, N. S.; Nocera, D. G. *Proc. Natl. Acad. Sci. U.S.A.* **2006**, *103*, 15729−15735.
(15) Norskov, J. K.; Rossmeisl, J.; Logadottir, A.; Lindqvist, L.; Kitchin, J. R.; Bligaard, T.; Jonsson, H. *J. Phys. Chem. B* **2004**, *108*, 17886−17892.
(16) Yang, X. F.; Baik, M. H. *J. Am. Chem. Soc.* **2004**, *126*, 13222−13223.
(17) Sundararajan, M.; Hillier, I. H.; Burton, N. A. *J. Phys. Chem. A* **2006**, *110*, 785−790.
(18) Bhattacharyya, S.; Stankovich, M. T.; Truhlar, D. G.; Gao, J. L. *J. Phys. Chem. A* **2007**, *111*, 5729−5742.
(19) Muckerman, J. T.; Polyansky, D. E.; Wada, T.; Tanaka, K.; Fujita, E. *Inorg. Chem.* **2008**, *47*, 1787−1802.
(20) Rauschnot, J. C.; Yang, C.; Yang, V.; Bhattacharyya, S. *J. Phys. Chem. B* **2009**, *113*, 8149−8157.
(21) Wang, T.; Brudvig, G. W.; Batista, V. S. *J. Chem. Theory Comput.* **2010**, *6*, 2395−2401.
(22) Wang, L. P.; Wu, Q.; Voorhis, T. V. *Inorg. Chem.* **2010**, *49*, 4543−4553.
(23) Barone, V.; Cossi, M. *J. Phys. Chem. A* **1998**, *102*, 1995−2001.
(24) Takano, Y.; Houk, K. N. *J. Chem. Theory Comput.* **2005**, *1*, 70−77.
(25) Cossi, M.; Barone, V.; Robb, M. A. *J. Chem. Phys.* **1999**, *111*, 5295−5302.
(26) Cammi, R.; Frediani, L.; Mennucci, B.; Ruud, K. *J. Chem. Phys.* **2003**, *119*, 5818−5827.
(27) Cammi, R.; Mennucci, B.; Tomasi, J. *J. Phys. Chem. A* **1999**, *103*, 9100−9108.
(28) Baldridge, K. K.; Jonas, V. *J. Chem. Phys.* **2000**, *113*, 7511−7518.
(29) Christiansen, O.; Mikkelsen, K. V. *J. Chem. Phys.* **1999**, *110*, 8348−8360.
(30) Cammi, R. *J. Chem. Phys.* **2009**, *131*, 164104.
(31) Caricato, M.; Scalmani, G.; Trucks, G. W.; Frisch, M. J. *J. Phys. Chem. Lett.* **2010**, *1*, 2369−2373.
(32) Caricato, M.; Mennucci, B.; Scalmani, G.; Trucks, G. W.; Frisch, M. J. *J. Chem. Phys.* **2010**, *132*, 084102.
(33) Becke, A. D. *J. Chem. Phys.* **1993**, *98*, 5648−5652.
(34) Perdew, J. P.; Burke, K.; Ernzerhof, M. *Phys. Rev. Lett.* **1996**, *77*, 3865−3868.
(35) Curtiss, L. A.; Raghavachari, K.; Redfern, P. C.; Pople, J. A. *J. Chem. Phys.* **1997**, *106*, 1063−1079.
(36) Curtiss, L. A.; Redfern, P. C.; Raghavachari, K.; Pople, J. A. *J. Chem. Phys.* **1998**, *109*, 42−55.
(37) Neese, F.; Hansen, A.; Wennmohs, F.; Grimme, S. *Acc. Chem. Res.* **2009**, *42*, 641−648.
(38) Boese, A. D.; Martin, J. M. L. *J. Chem. Phys.* **2004**, *121*, 3405−3416.
(39) Zhao, Y.; Schultz, N. E.; Truhlar, D. G. *J. Chem. Theory Comput.* **2006**, *2*, 364−382.
(40) Karton, A.; Tarnopolsky, A.; Lamere, J. F.; Schatz, G. C.; Martin, J. M. L. *J. Phys. Chem. A* **2008**, *112*, 12868−12886.
(41) Gutsev, G. L.; Bauschlicher, C. W. *J. Phys. Chem. A* **2003**, *107*, 4755−4767.
(42) Riley, K. E.; Merz, K. M. *J. Phys. Chem. A* **2007**, *111*, 6044−6053.
(43) Jensen, K. P.; Roos, B. O.; Ryde, U. *J. Chem. Phys.* **2007**, *126*, 014103.
(44) Cramer, C. J.; Truhlar, D. G. *Phys. Chem. Chem. Phys.* **2009**, *11*, 10757−10816.
(45) Born, M. *Z. Phys.* **1920**, *1*, 45−48.
(46) Kirkwood, J. *J. Chem. Phys.* **1934**, *2*, 767.
(47) Onsager, L. *J. Am. Chem. Soc.* **1936**, *58*, 1486−1493.
(48) Foresman, J. B.; Keith, T. A.; Wiberg, K. B.; Snoonian, J.; Frisch, M. J. *J. Phys. Chem.* **1996**, *100*, 16098−16104.
(49) Klamt, A.; Schuurmann, G. *J. Chem. Soc., Perkin Trans. 2* **1993**, 799−805.
(50) Rashin, A. A.; Honig, B. *J. Phys. Chem.* **1985**, *89*, 5588−5593.
(51) Cossi, M.; Rega, N.; Scalmani, G.; Barone, V. *J. Comput. Chem.* **2003**, *24*, 669−681.
(52) Cances, E.; Mennucci, B.; Tomasi, J. *J. Chem. Phys.* **1997**, *107*, 3032−3041.
(53) Cramer, C. J.; Truhlar, D. G. *Acc. Chem. Res.* **2008**, *41*, 760−768.
(54) Cramer, C. J.; Truhlar, D. G. *Chem. Rev.* **1999**, *99*, 2161−2200.
(55) Amovilli, C.; Mennucci, B. *J. Phys. Chem. B* **1997**, *101*, 1051−1057.
(56) Mongan, J.; Simmerling, C.; McCammon, J. A.; Case, D. A.; Onufriev, A. *J. Chem. Theory Comput.* **2007**, *3*, 156−169.
(57) Yang, P. K.; Lim, C. *J. Phys. Chem. B* **2008**, *112*, 14863−14868.
(58) Mouesca, J. M.; Chen, J. L.; Noodleman, L.; Bashford, D.; Case, D. A. *J. Am. Chem. Soc.* **1994**, *116*, 11898−11914.
(59) Li, J.; Fisher, C. L.; Chen, J. L.; Bashford, D.; Noodleman, L. *Inorg. Chem.* **1996**, *35*, 4694−4702.
(60) Baik, M. H.; Friesner, R. A. *J. Phys. Chem. A* **2002**, *106*, 7407−7412.
(61) Uudsemaa, M.; Tamm, T. *J. Phys. Chem. A* **2003**, *107*, 9997−10003.
(62) Lewis, A.; Bumpus, J. A.; Truhlar, D. G.; Cramer, C. J. *J. Chem. Educ.* **2004**, *81*, 596−604.
(63) Barone, V.; Rienzo, F. D.; Langella, E.; Menziani, M. C.; Regal, N.; Sola, M. *Proteins: Struct., Funct., Bioinf.* **2006**, *62*, 262−269.
(64) Speelman, A. L.; Gillmore, J. G. *J. Phys. Chem. A* **2008**, *112*, 5684−5690.
(65) Roy, L. E.; Jakubikova, E.; Guthrie, M. G.; Batista, E. R. *J. Phys. Chem. A* **2009**, *113*, 6745−6750.
(66) Winget, P.; Weber, E. J.; Cramer, C. J.; Truhlar, D. G. *Phys. Chem. Chem. Phys.* **2000**, *2*, 1231−1239.
(67) Fu, Y.; Liu, L.; Yu, H. Z.; Wang, Y. M.; Guo, Q. X. *J. Am. Chem. Soc.* **2005**, *127*, 7227−7234.
(68) am Busch, M. S.; Knapp, E. W. *J. Am. Chem. Soc.* **2005**, *127*, 15730−15737.

(69) Chiorescu, I.; Deubel, D. V.; Arion, V. B.; Keppler, B. K. *J. Chem. Theory Comput.* **2008**, *4*, 499−506.
(70) Jaque, P.; Marenich, A. V.; Cramer, C. J.; Truhlar, D. G. *J. Phys. Chem. C* **2007**, *111*, 5783−5799.
(71) Marenich, A. V.; Olson, R. M.; Chamberlin, A. C.; Cramer, C. J.; Truhlar, D. G. *J. Chem. Theory Comput.* **2007**, *3*, 2055−2067.
(72) Bryantsev, V. S.; Diallo, M. S.; Goddard, W. A. *J. Phys. Chem. A* **2009**, *113*, 9559−9567.
(73) Khaliullin, R. Z.; Bell, A. T.; Head-Gordon, M. *J. Chem. Phys.* **2008**, *128*, 184112.
(74) Khaliullin, R. Z.; Bell, A. T.; Head-Gordon, M. *Chem.—Eur. J.* **2009**, *15*, 851−855.
(75) Mo, Y.; Bao, P.; Gao, J. *Phys. Chem. Chem. Phys.* **2011**, *13*, 6760−6775.
(76) Fattebert, J. L.; Gygi, F. *J. Comput. Chem.* **2002**, *23*, 662−666.
(77) Scherlis, D. A.; Fattebert, J. L.; Gygi, F.; Cococcioni, M.; Marzari, N. *J. Chem. Phys.* **2006**, *124*, 074103.
(78) Galstyan, A.; Knapp, E. W. *J. Comput. Chem.* **2009**, *30*, 203−211.
(79) Berendsen, H. J. C.; Grigera, J. R.; Straatsma, T. P. *J. Phys. Chem.* **1987**, *91*, 6269−6271.
(80) Field, M. J.; Bash, P. A.; Karplus, M. *J. Comput. Chem.* **1990**, *11*, 700−733.
(81) Aaqvist, J.; Warshel, A. *Chem. Rev.* **1993**, *93*, 2523−2544.
(82) Gao, J. L.; Truhlar, D. G. *Annu. Rev. Phys. Chem.* **2002**, *53*, 467−505.
(83) Zeng, X. C.; Hu, H.; Hu, X. Q.; Cohen, A. J.; Yang, W. T. *J. Chem. Phys.* **2008**, *128*, 124510.
(84) Blumberger, J.; Bernasconi, L.; Tavernelli, I.; Vuilleumier, R.; Sprik, M. *J. Am. Chem. Soc.* **2004**, *126*, 3928−3938.
(85) Zeng, X. C.; Hu, H.; Hu, X. Q.; Yang, W. T. *J. Chem. Phys.* **2009**, *130*, 164111.
(86) Moens, J.; Seidel, R.; Geerlings, P.; Faubel, M.; Winter, B.; Blumberger, J. *J. Phys. Chem. B* **2010**, *114*, 9173−9182.
(87) Cheng, J.; Sulpizi, M.; Sprik, M. *J. Chem. Phys.* **2009**, *131*, 154504.
(88) Li, G. H.; Zhang, X. D.; Cui, Q. *J. Phys. Chem. B* **2003**, *107*, 8643−8653.
(89) Brunelle, P.; Rauk, A. *J. Phys. Chem. A* **2004**, *108*, 11032−11041.
(90) Riccardi, D.; Schaefer, P.; Cui, Q. *J. Phys. Chem. B* **2005**, *109*, 17715−17733.
(91) Rickard, G. A.; Berges, J.; Houee-Levin, C.; Rauk, A. *J. Phys. Chem. B* **2008**, *112*, 5774−5787.
(92) Kamerlin, S. C. L.; Haranczyk, M.; Warshel, A. *J. Phys. Chem. B* **2009**, *113*, 1253−1272.
(93) Reiss, H.; Heller, A. *J. Phys. Chem.* **1985**, *89*, 4207−4213.
(94) Kelly, C. P.; Cramer, C. J.; Truhlar, D. G. *J. Phys. Chem. B* **2007**, *111*, 408−422.
(95) Gomer, R.; Tryson, G. *J. Chem. Phys.* **1977**, *66*, 4413−4424.
(96) Frenkel, D.; Smit, B. *Understanding Molecular Simulation*, 2nd ed.; Academic Press: San Diego, CA, 2001.
(97) Metropolis, N.; Rosenbluth, A. W.; Rosenbluth, M. N.; Teller, A. H.; Teller, E. *J. Chem. Phys.* **1953**, *21*, 1087−1092.
(98) Ahlrichs, R.; Bar, M.; Haser, M.; Horn, H.; Kolmel, C. *Chem. Phys. Lett.* **1989**, *162*, 165−169.
(99) Schafer, A.; Klamt, A.; Sattel, D.; Lohrenz, J. C. W.; Eckert, F. *Phys. Chem. Chem. Phys.* **2000**, *2*, 2187−2193.
(100) Bondi, A. *J. Phys. Chem.* **1964**, *68*, 441−444.
(101) Andrae, D.; Haussermann, U.; Dolg, M.; Stoll, H.; Preuss, H. *Theor. Chim. Acta* **1990**, *77*, 123−141.
(102) Schafer, A.; Huber, C.; Ahlrichs, R. *J. Chem. Phys.* **1994**, *100*, 5829−5835.
(103) Dunning, T. H. *J. Chem. Phys.* **1989**, *90*, 1007−1023.
(104) Rappe, A. K.; Casewit, C. J.; Colwell, K. S.; Goddard, W. A.; Skiff, W. M. *J. Am. Chem. Soc.* **1992**, *114*, 10024−10035.
(105) Ryckaert, J. P.; Ciccotti, G.; Berendsen, H. J. C. *J. Comput. Phys.* **1977**, *23*, 327−341.
(106) Lamoureux, G.; Roux, B. *J. Chem. Phys.* **2003**, *119*, 3025−3039.
(107) Lamoureux, G.; MacKerell, A. D.; Roux, B. *J. Chem. Phys.* **2003**, *119*, 5185−5197.
(108) Kathmann, S. M.; Kuo, I.-F. W.; Mundy, C. J.; Schenter, G. K. *J. Phys. Chem. B* **2011**, *115*, 4369−4377.
(109) Harder, E.; Roux, B. *J. Chem. Phys.* **2008**, 129.
(110) Brooks, B. R.; Bruccoleri, R. E.; Olafson, B. D.; States, D. J.; Swaminathan, S.; Karplus, M. *J. Comput. Chem.* **1983**, *4*, 187−217.
(111) Shao, Y.; et al. *Phys. Chem. Chem. Phys.* **2006**, *8*, 3172−3191.
(112) Woodcock, H. L.; Hodoscek, M.; Gilbert, A. T. B.; Gill, P. M. W.; Schaefer, H. F.; Brooks, B. R. *J. Comput. Chem.* **2007**, *28*, 1485−1502.
(113) Difley, S.; Wang, L. P.; Yeganeh, S.; Yost, S. R.; Voorhis, T. V. *Acc. Chem. Res.* **2010**, *43*, 995−1004.
(114) *CRC Handbook of Chemistry and Physics*, 91st ed.; CRC Press: Boca Raton, FL2010 (accessed February 8, 2011).
(115) Wu, Z. J.; Kawazoe, Y. *Chem. Phys. Lett.* **2006**, *423*, 81−86.
(116) Yang, Y.; Weaver, M. N.; Merz, K. M. *J. Phys. Chem. A* **2009**, *113*, 9843−9851.
(117) Wang, L. P.; Van Voorhis, T. *J. Chem. Phys.* **2010**, *133*, 231101.